VNU Journal of Mathematics – Physics, Vol. 29, No. 3 (2013) 14-31

Buckling Analysis of Functionally Graded Annular Spherical Shells and Segments Subjected to Mechanic Loads

Dao Huy Bich[1], Nguyen Thi Phuong[2,*]

[1]*Vietnam National University, Hanoi, 144 Xuan Thuy, Cau Giay, Hanoi, Vietnam*
[2]*University of Transport Technology, 54 Trieu Khuc, Thanh Xuan, Hanoi, Vietnam*

Received 15 August 2013
Revised 05 September 2013; Accepted 10 September 2013

Abstract: An analytical approach is presented to investigate the buckling of functionally graded annular spherical segments subjected to compressive load and radial pressure. Based on the classical thin shell theory, the governing equations of functionally graded annular spherical segments are derived. Approximate solutions are assumed to satisfy the simply supported boundary condition of segments and Galerkin method is applied to obtain closed-form relations of bifurcation type of buckling loads. Numerical results are given to evaluate effects of inhomogeneous and dimensional parameters to the buckling of structure.

Keywords: Functionally graded material; annular spherical segment; critical buckling load.

1. Introduction

The static and dynamic behavior of spherical shaped structures made of different materials attracted special attention of many researchers in long time. Budiansky and Roth [1] studied axisymmetrical dynamic buckling of clamped shallow isotropic spherical shells. Their well-known results have received considerable attention in the literature. Huang [2] considered the unsymmetrical buckling of thin shallow spherical shells under external pressure. He pointed out that unsymmetrical deformation may be the source of discrepancy in critical pressures between axisymmetrical buckling theory and experiment. The static buckling behavior of shallow spherical caps under uniform pressure loads was analyzed by Tillman [3]. Results on the dynamic buckling of clamped shallow spherical shells subjected to axisymmetric and nearly axisymmetric step-pressure loads using a digital computer program were given by Ball and Burt [4]. Kao and Perrone [5] reported the dynamic buckling of isotropic axisymmetrical spherical caps with initial imperfection. Two types of loading are considered, in this paper, namely, step loading with infinite duration and right triangular pulse. Based on an assumed two-term mode shape for the lateral displacement, Ganapathi and Varadan [6] investigated

* Corresponding author. Tel.: 84- 1674829686
Email: nguyenthiphuong@utt.edu.vn

the problem of dynamic buckling of orthotropic shallow spherical shells under instantaneously applied uniform step-pressure load of infinite duration. Nonlinear free vibration response, static response under uniformly distributed load, and the maximum transient response under uniformly distributed step load of orthotropic thin spherical caps on elastic foundations were obtained by Dumir [7]. Static and dynamic snap through buckling of orthotropic spherical caps based on the classical thin shell theory and Reissener's shallow shell assumptions were considered by Chao and Lin [8] using finite difference method. Buckling and postbuckling behaviors of laminated spherical caps subjected to uniform external pressure were analyzed by Xu [9] and Muc [10]. The former employed non-linear shear deformation theory and a Fourier-Bessel series solution to determine load – deflection curves of spherical shell under axisymmetric deformation, whereas the latter applied the classical shell theory and Rayleigh–Ritz procedure to obtain upper and lower pressures and postbuckling equilibrium paths without considering axisymmetry. Ganapathi and Varadan analyzed the dynamical buckling of laminated anisotropic spherical caps using the finite element method [11]. A static and dynamic non-linear axisymmetric analysis of thick shallow spherical and conical orthotropic caps was reported by Dube et al. [12] employing Galerkin method and the first order shear deformation theory. Also, Nie [13] proposed the asymptotic iteration method to treat non-linear buckling of externally pressurized isotropic shallow spherical shells with various boundary conditions incorporating the effects of imperfection, edge elastic restraint and elastic foundation. There were several investigations on the buckling of spherical shells under mechanical or thermal load taking into account initial imperfection such as studies by Eslami et al. [14] and Shahsiah and Eslami [15]. Wunderlich and Albertin [16] also studied the static buckling behavior of isotropic imperfect spherical shells. New design rules in their work for these shells were developed, which take into account relevant details like boundary conditions, material properties and imperfections. Li et al. [17] adopted the modified iteration method to solve nonlinear stability problem of shear deformable isotropic shallow spherical shells under uniform external pressure.

In recent years, many authors have focused on the mechanic and thermal behavior of functionally graded (FGM) spherical panels and shells. Shahsiah et al. [18] presented an analytical approach to study the instability of FGM shallow spherical shells under three types of thermal loading including uniform temperature rise, linear radial temperature, and nonlinear radial temperature. Prakash et al. [19] obtained results on the nonlinear axisymmetric dynamic buckling behavior of clamped FGM spherical caps. Also, the dynamic stability characteristics of FGM shallow spherical shells were considered by Ganapathi [20] using the finite element method. In his study, the geometric nonlinearity is assumed only in the meridional direction in strain– displacement relations. Bich [21] studied the nonlinear buckling of FGM shallow spherical shells using an analytical approach and the geometrical nonlinearity was considered in all strain–displacement relations. By using Galerkin procedure and Runge–Kutta method, Bich and Hoa [22] analyzed the nonlinear vibration of FGM shallow spherical shells subjected to harmonic uniform external pressures. Recently, Bich and Tung [23] reported an analytical investigation on the nonlinear axisymmetrical response of FGM shallow spherical shells under uniform external pressure taking the effects of temperature conditions into consideration. Shahsiah et al. [24] used an analytical approach to investigate thermal linear instability of FGM deep spherical shells under three types of thermal loads using the first order shell theory based on Sander

nonlinear kinematic relations. Bich et al. [25] investigated nonlinear static and dynamic buckling analysis of functionally graded shallow spherical shells including temperature effects.

Other special structural FGM panels are also interested by some authors in recent years. Aghdam et al.[26] investigated bending of moderately thick clamped FG conical panels subjected to uniform and nonuniform distributed loadings. First-order shear deformation theory (FSDT) is applied to drive the governing equations of the problem and solved its by using the Extended Kantorovich Method (EKM). Bich et al. [27] proposed an analytical approach to investigate the linear buckling of FGM conical panels subjected to axial compression, external pressure and the combination of these loads. Base on the classical thin shell theory, the equilibrium and linear stability equations in terms of displacement components are derived and the approximate analytical solutions are assumed to satisfy simply supported boundary conditions and Galerkin method.

Annular spherical segments become popularly in engineering designs. However, the special geometrical shape of this structure is a big difficulty to find the explicit solution form of buckling loads. This paper presents an analytical approach to investigate buckling of functionally graded annular spherical segments subjected to compressive load and radial pressure. An approximate solution form is presented and the explicit solution form is obtained for critical buckling loads of segments.

2. Functionally graded annular spherical segment

Consider a FGM annular spherical segment or a FGM open annular spherical shell limited by two **meridians and two** parallels of a spherical shell, with thickness h, open angle of two meridional planes β, curvature radius R, rise H, radii of upper and lower bases r_0 and r_1 respectively, as shown in Fig. 1. It is defined in coordinate system (φ,θ,z), where φ and θ are in the medional and circumferential directions of the shell respectively and z is perpendicular to the middle surface positive in- ward. Particularly, the segment with $\beta = 2\pi$ becomes an annular spherical shell.

Assume that the shell is made from a mixture of ceramic and metal constituents and the effective material properties vary continuously along the thickness by the power law distribution.

$$V_c = V_c(z) = \left(\frac{2z+h}{2h}\right)^k,\ V_m = V_m(z) = 1 - V_c(z), \tag{1}$$

where $k \geq 0$ is the volume-fraction index; the subscripts m and c refer to the metal and ceramic constituents respectively.

According to the mentioned law, the Young modulus can be expressed in the form

$$E(z) = E_m V_m + E_c V_c = E_m + (E_c - E_m)\left(\frac{2z+h}{2h}\right)^k, \tag{2}$$

and the Poisson ratio ν is assumed to be constant.

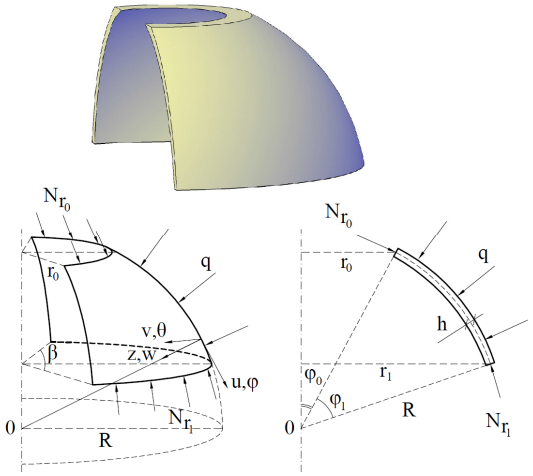

Fig. 1. Configuration of an annular spherical segment.

3. Formulation of the problem

For a shallow annular spherical shell it is convenient to introduce an additional variable *r* defined by the relation $r = R\sin\varphi$, where r is the radius of the parallel circle with the base of shell. If the rise *H* of shell is much smaller than the lower base radius r_1 we can take $\cos\varphi \approx 1$ and $Rd\varphi = dr$, such that points of the middle surface may be referred to coordinates *r* and θ.

The strains across the shell thickness at a distance z from the mid-surface are:

$$\varepsilon_r = \varepsilon_{rm} - z\chi_r, \qquad \varepsilon_\theta = \varepsilon_{\theta m} - z\chi_\theta, \qquad \gamma_{r\theta} = \gamma_{r\theta m} - 2z\chi_{r\theta}, \tag{3}$$

where ε_{rm} and $\varepsilon_{\theta m}$ are the normal strains, $\gamma_{r\theta m}$ is the shear strain at the middle surface of the annular spherical segment, whereas χ_r, χ_θ and $\chi_{r\theta}$ are the change of curvatures and twist that are related to the displacement components u, v and w of the middle surface points along meridional, circumferential and radial direction, respectively, as

$$\begin{aligned} &\varepsilon_{rm} = \frac{\partial u}{\partial r} - \frac{w}{R} + \frac{1}{2}\left(\frac{\partial w}{\partial r}\right)^2, \quad \varepsilon_{\theta m} = \frac{1}{r}\left(\frac{\partial v}{\partial \theta} + u\right) - \frac{w}{R} + \frac{1}{2r^2}\left(\frac{\partial w}{\partial \theta}\right)^2, \\ &\gamma_{r\theta m} = r\frac{\partial}{\partial r}\left(\frac{v}{r}\right) + \frac{1}{r}\frac{\partial u}{\partial \theta} + \frac{1}{r}\frac{\partial w}{\partial r}\frac{\partial w}{\partial \theta}. \end{aligned} \tag{4}$$

$$\chi_r = \frac{\partial^2 w}{\partial r^2}, \quad \chi_\theta = \frac{1}{r^2}\frac{\partial^2 w}{\partial \theta^2} + \frac{1}{r}\frac{\partial w}{\partial r}, \quad \chi_{r\theta} = \frac{1}{r}\frac{\partial^2 w}{\partial r \partial \theta} - \frac{1}{r}\frac{\partial w}{\partial r}. \tag{5}$$

The stress – strain relationships for an annular spherical segment are defined by the Hooke law

$$(\sigma_r,\sigma_\theta)=\frac{E(z)}{1-\upsilon^2}\left[(\varepsilon_x,\ \varepsilon_\theta)+\upsilon(\varepsilon_\theta,\ \varepsilon_x)\right],\quad \sigma_{r\theta}=\frac{E(z)}{2(1+\upsilon)}\gamma_{r\theta}, \tag{6}$$

The force and moment resultants of an FGM annular spherical segment are expressed in terms of the stress components through the thickness as

$$\left\{(N_r,\ N_\theta,\ N_{r\theta}),(M_r,\ M_\theta,M_{r\theta})\right\}=\int_{-h/2}^{h/2}\{\sigma_r,\ \sigma_\theta,\ \sigma_{r\theta}\}(1,\ z)dz \tag{7}$$

Introduction of Eqs. (2), (3) and (6) in Eq.(7) gives the constitutive relations as

$$\begin{aligned}
(N_r,M_r)&=\frac{(E_1,E_2)}{1-\nu^2}(\varepsilon_r+\nu\varepsilon_\theta)-\frac{(E_2,E_3)}{1-\nu^2}(\chi_r+\nu\chi_\theta),\\
(N_\theta,M_\theta)&=\frac{(E_1,E_2)}{1-\nu^2}(\varepsilon_\theta+\nu\varepsilon_r)-\frac{(E_2,E_3)}{1-\nu^2}(\chi_\theta+\nu\chi_r),\\
(N_{r\theta},M_{r\theta})&=\frac{(E_1,E_2)}{2(1+\nu)}\gamma_{r\theta}-\frac{(E_2,E_3)}{1+\nu}\chi_{r\theta},
\end{aligned} \tag{8}$$

where

$$E_1=\int_{-h/2}^{h/2}E(z)dz=\left(E_m+\frac{E_c-E_m}{k+1}\right)h,\quad E_2=\int_{-h/2}^{h/2}E(z)zdz=\frac{(E_c-E_m)kh^2}{2(k+1)(k+2)},$$

$$E_3=\int_{-h/2}^{h/2}E(z)z^2dz=\left[\frac{E_m}{12}+(E_c-E_m)\left(\frac{1}{k+3}-\frac{1}{k+2}+\frac{1}{4k+4}\right)\right]h^3,$$

The nonlinear equilibrium equations of a perfect annular spherical segment according to the classical shell theory are [28]

$$\begin{aligned}
&\frac{\partial N_r}{\partial r}+\frac{1}{r}\frac{\partial N_{r\theta}}{\partial\theta}+\frac{N_r-N_\theta}{r}=0,\\
&\frac{\partial N_{r\theta}}{\partial r}+\frac{1}{r}\frac{\partial N_\theta}{\partial\theta}+\frac{2N_{r\theta}}{r}=0,\\
&\frac{\partial^2 M_r}{\partial r^2}+\frac{2}{r}\frac{\partial M_r}{\partial r}+2\left(\frac{1}{r}\frac{\partial^2 M_{r\theta}}{\partial r\partial\theta}+\frac{1}{r^2}\frac{\partial M_{r\theta}}{\partial\theta}\right)+\frac{1}{r^2}\frac{\partial^2 M_\theta}{\partial\theta^2}-\frac{1}{r}\frac{\partial M_\theta}{\partial r}+\frac{1}{R}(N_r+N_\theta)\\
&\qquad N_r\frac{\partial^2 w}{\partial r^2}-2N_{r\theta}\left(\frac{1}{r^2}\frac{\partial w}{\partial\theta}-\frac{1}{r}\frac{\partial^2 w}{\partial r\partial\theta}\right)+N_\theta\left(\frac{1}{r}\frac{\partial w}{\partial r}+\frac{1}{r^2}\frac{\partial^2 w}{\partial\theta^2}\right)+q=0.
\end{aligned} \tag{9}$$

Stability equations of FGM annular spherical segment may be established by the adjacent equilibrium criterion [28]. It is assumed that equilibrium state of the FGM annular spherical segment under applied load is represented by displacement components u_0, v_0 and w_0. The state of adjacent equilibrium differs that of stable equilibrium by u_1, v_1 and w_1, and the total displacement component of a neighboring configuration are

$$u = u_0 + u_1,\ v = v_0 + v_1,\ w = w_0 + w_1. \tag{10}$$

Similarly, the force and moment resultants of a neighboring state are represented by

$$N_r = N_{r0} + N_{r1},\ N_\theta = N_{\theta 0} + N_{\theta 1},\ N_{r\theta} = N_{r\theta 0} + N_{r\theta 1}. \tag{11}$$

$$M_r = M_{r0} + M_{r1},\ M_\theta = M_{\theta 0} + M_{\theta 1},\ M_{r\theta} = M_{r\theta 0} + M_{r\theta 1}. \tag{12}$$

where terms with 0 subscripts derive the force and moment resultants corresponding to u_0, v_0, w_0 displacements and those with 1 subscripts represent the portions of increments corresponding to u_1, v_1, w_1 .

Introduction of Eqs. (10), (11) and (12) into Eq.(9) and subtracting from the resulting equations terms relating to stable equilibrium state, neglecting nonlinear terms in u_1, v_1, w_1 or their counterparts in the form of N_{r1}, N_{r0} etc yield

$$\begin{aligned}
&\frac{\partial N_{r1}}{\partial r} + \frac{1}{r}\frac{\partial N_{r\theta 1}}{\partial \theta} + \frac{N_{r1} - N_{\theta 1}}{r} = 0,\\
&\frac{\partial N_{r\theta 1}}{\partial r} + \frac{1}{r}\frac{\partial N_{\theta 1}}{\partial \theta} + \frac{2N_{r\theta 1}}{r} = 0,\\
&\frac{\partial^2 M_{r1}}{\partial r^2} + \frac{2}{r}\frac{\partial M_{r1}}{\partial r} + 2\left(\frac{1}{r}\frac{\partial^2 M_{r\theta 1}}{\partial r \partial \theta} + \frac{1}{r^2}\frac{\partial M_{r\theta 1}}{\partial \theta}\right) + \frac{1}{r^2}\frac{\partial^2 M_{\theta 1}}{\partial \theta^2} - \frac{1}{r}\frac{\partial M_{\theta 1}}{\partial r} + \frac{1}{R}\left(N_{r1} + N_{\theta 1}\right)\\
&\qquad N_{r0}\frac{\partial^2 w_1}{\partial r^2} + 2\frac{N_{r\theta 0}}{r}\frac{\partial^2 w_1}{\partial r \partial \theta} + \frac{N_{\theta 0}}{r^2}\frac{\partial^2 w_1}{\partial \theta^2} + \frac{N_{\theta 0}}{r}\frac{\partial w_1}{\partial r} - 2\frac{N_{\theta 0}}{r^2}\frac{\partial w_1}{\partial \theta} = 0.
\end{aligned} \tag{13}$$

where the force and moment resultants relating to stability state are

$$\left(N_{r1}, M_{r1}\right) = \frac{\left(E_1, E_2\right)}{1-\nu^2}\left(\varepsilon_{r1} + \nu\varepsilon_{\theta 1}\right) - \frac{\left(E_2, E_3\right)}{1-\nu^2}\left(\chi_{r1} + \nu\chi_{\theta 1}\right),\ \text{etc.} \tag{14}$$

in which

$$\varepsilon_{r1} = \frac{\partial u_1}{\partial r} - \frac{w_1}{R},\ \varepsilon_{\theta 1} = \frac{1}{r}\left(\frac{\partial v_1}{\partial \theta} + u_1\right) - \frac{w_1}{R},\ \gamma_{r\theta 1} = r\frac{\partial}{\partial r}\left(\frac{v_1}{r}\right) + \frac{1}{r}\frac{\partial u_1}{\partial \theta}, \tag{15}$$

$$\chi_{r1} = \frac{\partial^2 w_1}{\partial r^2},\ \chi_{\theta 1} = \frac{1}{r^2}\frac{\partial^2 w_1}{\partial \theta^2} + \frac{1}{r}\frac{\partial w_1}{\partial r},\ \chi_{r\theta 1} = \frac{1}{r}\frac{\partial^2 w_1}{\partial r \partial \theta} - \frac{1}{r}\frac{\partial w_1}{\partial r}. \tag{16}$$

The considered FGM annular spherical segment or the open annular spherical shell is assumed to be subjected to combination of external pressure q (Pascal) uniformly distributed on the outer surface

and uniformly compressive load P (where $P=ph$, p (Pascal)) acting on the two end edges in the tangential direction to meridian of the segment. Therefore the prebuckling state will be symmetric and determined by membrane forces N_{r0}, $N_{\theta 0}$ and $N_{r\theta 0}=0.$

Similarly with the approach to open conical shells [27, 30] projecting all external and internal force acting on an element of the annular segment onto the symmetry of the annular spherical shell yields

$$r_0\beta ph\sin\varphi_0 + r\beta N_{r0}\sin\varphi + \int_0^{\beta}\int_{\varphi_0}^{\varphi} q\cos\varphi R\sin\varphi d\theta R d\varphi = 0,$$

and onto the z-direction of the shell

$$\frac{N_{r0}}{R_1}+\frac{N_{\theta 0}}{R_2}+q=0,$$

where $r_0 = R\sin\varphi_0$, $r = R\sin\varphi$, $R_1 = R_2 = R.$

Establishing some calculation leads to

$$N_{r0} = -\frac{qR}{2}\left(1-\frac{\sin^2\varphi_0}{\sin^2\varphi}\right) - ph\frac{r_0\sin\varphi_0}{R\sin^2\varphi},$$

$$N_{\theta 0} = -N_{r0} - Rq = -\frac{qR}{2}\left(1+\frac{\sin^2\varphi_0}{\sin^2\varphi}\right) + ph\frac{r_0\sin\varphi_0}{R\sin^2\varphi},$$

and replacing $\sin\varphi_0 = \frac{r_0}{R}$, $\sin\varphi = \frac{r_1}{R}$, yields

$$N_{r0} = -qR\frac{\left(r^2-r_0^2\right)}{2r^2} - ph\frac{r_0^2}{r^2},\ N_{\theta 0} = -qR\frac{\left(r^2+r_0^2\right)}{2r^2} + ph\frac{r_0^2}{r^2},\ N_{r\theta 0}=0. \tag{17}$$

Substitution of Eqs. (14)-(17) into Eq.(13) gives stability equations in terms of displacement increments as

$$l_{11}(u_1)+l_{12}(v_1)+l_{13}(w_1)=0, \tag{18}$$

$$l_{21}(u_1)+l_{22}(v_1)+l_{23}(w_1)=0, \tag{19}$$

$$l_{31}(u_1)+l_{32}(v_1)+l_{33}(w_1)+ql_{34}(w_1)+pl_{35}(w_1)=0. \tag{20}$$

where the detail of operators l_{ij} are displayed in Appendix A.

The edges of annular spherical segment are assumed to be free simply supported and associated boundary conditions are

$$\begin{aligned} &v_1 = 0,\ \mathrm{w}_1 = 0,\ M_{r1} = 0,\ \mathrm{N}_{r1} = 0 \quad at \quad r = r_0,\ r = r_1, \\ &u_1 = 0,\ \mathrm{w}_1 = 0,\ M_{\theta 1} = 0,\ \mathrm{N}_{\theta 1} = 0 \ at \quad \theta = 0,\ \theta = \beta, \end{aligned} \tag{21}$$

From boundary conditions (21) approximate solutions for Eqs.(18) –(20) are assumed as

$$\begin{aligned} u_1 &= U\cos\frac{m\pi(r-r_0)}{r_1-r_0}\sin\frac{n\pi\theta}{\beta}, \\ v_1 &= \mathrm{V}\sin\frac{m\pi(r-r_0)}{r_1-r_0}\cos\frac{n\pi\theta}{\beta}, \\ \mathrm{w}_1 &= \mathrm{W}\sin\frac{m\pi(r-r_0)}{r_1-r_0}\sin\frac{n\pi\theta}{\beta}. \end{aligned} \tag{22}$$

where *m, n* are numbers of half waves in meridional and circumferential direction, respectively. With the chosen expression of displacement increments (22) the condition at $r = r_0; r_1 : v_1 = 0,$ $w_1 = 0$ are satisfied identically but $N_{r1} = 0$ and $M_{r1} = 0$ are satisfied approximately in average sense.

Otherwise, as in Ref.[18] instead of conditions $N_{r1} = 0$ and $M_{r1} = 0$ at $r = r_0; r_1$ one can use approximated conditions $\frac{\partial u_1}{\partial r} = 0$ and $\frac{\partial^2 w_1}{\partial r^2} = 0$ at $r = r_0; r_1$ which are satisfied identically with the chosen displacement increments (22). About boundary conditions at $\theta = 0; \beta$ all conditions are satisfied identically with the chosen expressions (22).

Due to $r_0 \le r \le r_1$ and for sake of convenience in integration, Eqs. (18, 19) are multiplied by r^2 and Eq. (20) by r^3.

Subsequently, introduction of solutions (22) into obtained equations and applying Galerkin method for the resulting, that are

$$\begin{aligned} &\int_{r_0}^{r_1}\int_{0}^{\beta} R_1\cos\frac{m\pi(r-r_0)}{r_1-r_0}\sin\frac{n\pi\theta}{\beta}\,r\,dr\,d\theta = 0, \\ &\int_{r_0}^{r_1}\int_{0}^{\beta} R_2\sin\frac{m\pi(r-r_0)}{r_1-r_0}\cos\frac{n\pi\theta}{\beta}\,r\,dr\,d\theta = 0, \\ &\int_{r_0}^{r_1}\int_{0}^{\beta} R_3\sin\frac{m\pi(r-r_0)}{r_1-r_0}\sin\frac{n\pi\theta}{\beta}\,r\,dr\,d\theta = 0. \end{aligned} \tag{23}$$

where R_1, R_2, R_3 are the left hand sides of Eqs. (18)-(20) after theses equations are multiplied by r^2, r^2 and r^3, respectively, and substituted into by solutions (22), we obtain the following equations

$$\begin{aligned} &a_{11}U + a_{12}V + a_{13}\mathrm{W} = 0, \\ &a_{21}U + a_{22}V + a_{23}\mathrm{W} = 0, \\ &a_{31}U + a_{32}V + \left(a_{33} + \mathrm{a}_{34}\mathrm{q}^{*} + \mathrm{a}_{35}\mathrm{p}^{*}\right)\mathrm{W} = 0. \end{aligned} \tag{24}$$

where the detail of coefficient a_{ij} and p^{*}, q^{*} notation may be found in Appendix B:

Because the solutions (22) are nontrivial, the determinant of coefficient matrix of Eq. (24) must be zero

$$\begin{vmatrix} a_{11} & a_{12} & a_{13} \\ a_{21} & a_{22} & a_{23} \\ a_{31} & a_{32} & a_{33} + \mathrm{a}_{34}\mathrm{q}^{*} + \mathrm{a}_{35}\mathrm{p}^{*} \end{vmatrix} = 0 \tag{25}$$

Solving Eq. (25) for p^{*} and q^{*} yields

$$\mathrm{a}_{34}\mathrm{q}^{*} + \mathrm{a}_{35}\mathrm{p}^{*} = \frac{a_{31}\left(a_{12}a_{23} - a_{13}a_{22}\right) + a_{32}\left(a_{13}a_{21} - a_{11}a_{23}\right) + a_{33}\left(a_{11}a_{22} - a_{12}a_{21}\right)}{\left(a_{12}a_{21} - a_{11}a_{22}\right)} \tag{26}$$

Eq. (26) is used for determining the buckling loads of FGM annular spherical segment under uniform compressive load, external pressure and combined loads. For given values of the material and geometrical properties of the FGM segment, critical buckling loads are determined by minimizing loads with respect to values of m, n.

By introducing parameter $\gamma = \dfrac{\mathrm{p}^{*}}{\mathrm{q}^{*}}$, Eq. (26) becomes

$$\mathrm{q}^{*} = \frac{a_{31}\left(a_{12}a_{23} - a_{13}a_{22}\right) + a_{32}\left(a_{13}a_{21} - a_{11}a_{23}\right) + a_{33}\left(a_{11}a_{22} - a_{12}a_{21}\right)}{\left(a_{12}a_{21} - a_{11}a_{22}\right)\left(\mathrm{a}_{34} + \mathrm{a}_{35}\gamma\right)} \tag{27}$$

4. Results and discussion

To validate the present study, the present critical buckling loads of shallow spherical caps are compared with other results.

Table 1 shows the present results in comparison with those presented by Timoshenko and Gere [29]. In this comparison, the critical buckling loads of the homogeneous shallow spherical caps with simply supported movable edges under radial pressure. The Young modulus of Aluminum is $E = 70\left(GPa\right)$. The Poisson's ratio is chosen to be 0.3.

The comparison of critical buckling loads of FGM shallow spherical caps under radial pressure with the results of Bich [21] is shown in table 2. The combination of materials consists of aluminum $E_m = 70(GPa)$ and alumina $E_c = 380(GPa)$. The Poisson's ratio is chosen to be 0.3 for simplicity.

As can be seen in table 1 and 2, the very good agreements are obtained in these comparison studies.

Table 1. Comparison of critical buckling loads (q_{cr} x10^1) (Mpa) for homogeneous shallow spherical caps under radial pressure $q_{cr} = \dfrac{2Eh^2}{R^2\sqrt{3(1-\nu^2)}}$

R/h	800	1000	1200	1500	2000
Timoshenko and Gere[29]	1.9065	0.8473	0.5884	0.3766	0.2118
Present	1.9054 (15, 1)	0.8474 (18, 1)	0.5882 (20, 1)	0.3767 (22, 1)	0.2118 (26, 1)

Table 2. Comparison of critical buckling loads (q_{cr} x10) (Mpa) with Bich [21] for FGM shallow spherical caps under radial pressure $q_{cr} = 4\left(\dfrac{h}{R}\right)^2\sqrt{\dfrac{\left(\overline{E_1}\,\overline{E_3} - \overline{E_2^2}\right)}{1-\nu^2}}$

R/h	k	Bich [21]	Present
400			
	0	2.8748	2.8808 (12, 1)
	1	1.5618	1.5617 (12, 1)
	2	1.2109	1.2111 (12, 1)
600			
	0	1.2777	1.2771 (7, 1)
	1	0.6941	0.6944 (15, 1)
	2	0.5382	0.5386 (15, 1)
800			
	0	0.7187	0.7190 (16, 1)
	1	0.3904	0.3904 (17, 1)
	2	0.3027	0.3027 (17, 1)

To illustrate the proposed approach to annular spherical segment s, the segment s considered here are simply supported at all its edges. The FG material consists of aluminum $E_m = 70(GPa)$ and alumina $E_c = 380(GPa)$,the Poisson's ratio is chosen to be 0.3.

Table 3. Effects of open angle β, volume fraction index *k* and ratio *R/h* on the critical buckling loads p_{cr} (GPa) of annular spherical segment s under compressive load

R/h	$\beta(^o)$	15	30	45	60	75	90	360
	k	$(r_o/R=0.2,\ r_1/R=0.5)$						
800								
	0	2.3476 [b]	1.3859 [a]	1.2404 [a]	1.1942 [a]	1.1736 [a]	1.1625 [a]	1.1395 [a]
	1	1.2117 [c]	0.7485 [a]	0.6726 [a]	0.6485 [a]	0.6378 [a]	0.6320 [a]	0.6200 [a]
	5	0.7671 [b]	0.4508 [a]	0.4035 [a]	0.3885 [a]	0.3818 [a]	0.3783 [a]	0.3708 [a]
	10	0.6810 [b]	0.3903 [a]	0.3484 [a]	0.3351 [a]	0.3292 [a]	0.3260 [a]	0.3194 [a]
1000								
	0	1.6423 [c]	1.0678 [b]	0.9857 [b]	0.9588 [b]	0.9467 [b]	0.9402 [b]	0.9252 [a]
	1	0.8518 [c]	0.5709 [b]	0.5285 [b]	0.5146 [b]	0.5083 [b]	0.5050 [b]	0.4979 [b]
	5	0.5367 [c]	0.3478 [b]	0.3211 [b]	0.3123 [b]	0.3083 [a]	0.3057 [a]	0.3002 [a]
	10	0.4771 [c]	0.3031 [b]	0.2762 [a]	0.2666 [a]	0.2623 [a]	0.2600 [a]	0.2551 [a]
1200								
	0	1.2497 [c]	0.8668 [b]	0.8044 [b]	0.7839 [b]	0.7746 [b]	0.7697 [b]	0.7592 [b]
	1	0.6562 [c]	0.4699 [c]	0.4380 [b]	0.4273 [b]	0.4225 [b]	0.4199 [b]	0.4144 [b]
	5	0.4077 [c]	0.2817 [c]	0.2614 [b]	0.2548 [b]	0.2518 [b]	0.2501 [b]	0.2468 [b]
	10	0.3596 [c]	0.2429 [c]	0.2250 [b]	0.2191 [b]	0.2165 [b]	0.2150 [b]	0.2121 [b]
1500								
	0	0.9122 [d]	0.6739 [c]	0.6370 [c]	0.6247 [c]	0.6191 [c]	0.6161 [c]	0.6097 [c]
	1	0.4786 [d]	0.3637 [c]	0.3445 [c]	0.3381 [c]	0.3352 [c]	0.3336 [c]	0.3303 [c]
	5	0.2976 [d]	0.2192 [c]	0.2072 [c]	0.2032 [c]	0.2014 [c]	0.2004 [c]	0.1983 [c]
	10	0.2626 [d]	0.1898 [d]	0.1792 [c]	0.1756 [c]	0.1740 [c]	0.1731 [c]	0.1710 [b]

The buckling mode shape: [a]=(5, 1) [b]=(6, 1) [c]=(7, 1) [d]=(8, 1)

Effects of angle of two meridian planes β, volume fraction index k and ratio *R/h* on the critical buckling loads of annular spherical segment s under compressive load are shown in Table 3. The results show that critical buckling loads decrease when the value of these parameters increases.

Table 4 shows the effects of ratio r_o/R and r_1/R on the critical buckling load p_{cr} (GPa) of annular spherical segment under compressive load. The critical load of annular spherical segment increases when the ratio of r_1/R increases, conversely, it decreases when the ratio r_0/R increase.

Table 4. Effects of ratio r_o/R and r_1/R on the critical buckling load p_{cr} (GPa) of annular spherical segment under compressive load $(k=1,\ R/h=1000,\ \beta=45^o)$

r_0/R	r_1/R				
	0.3	0.35	0.4	0.45	0.5
0.1	0.8395 (4, 1)	1.0812 (5, 1)	1.3615 (6, 1)	1.6802 (7, 1)	2.0368 (8, 1)
0.15	0.3893 (3, 1)	0.4949 (4, 1)	0.6180 (5, 1)	0.7584 (6, 1)	0.9159 (7, 1)
0.2	0.2384 (2, 1)	0.2959 (3, 1)	0.3635 (4, 1)	0.4411 (5, 1)	0.5285 (6, 1)
0.25	0.1720 (1, 1)	0.2072 (2, 1)	0.2490 (3, 1)	0.2974 (4, 1)	0.3523 (5, 1)

Table 5 shows the effects of angle of two median planes β, volume fraction index *k* and ratio *R/h* on the critical buckling loads of annular spherical segments under radial pressure. It is evident that critical buckling loads decrease when the volume of these parameter increases, similarly in the case of segments under compressive load.

Table 5. Effects of open angle β, volume fraction index k and ratio *R/h* on the critical buckling loads q_{cr} x 10^4 (GPa) of annular spherical segments under radial pressure

R/h	$\beta\left(^o\right)$	15	30	45	60	90	360
	k	$\left(r_o/R=0.2,\ r_1/R=0.5\right)$					
800							
	0	6.6609(1, 2)	5.9334(1, 3)	5.9807(1, 5)	5.9334(1, 6)	5.9334(1, 9)	8.8174 (4, 15)
	1	3.5206(1, 2)	3.2771(1, 3)	3.2494(1, 5)	3.2771(1, 6)	3.2494(1, 10)	4.8485 (5, 15)
	5	2.1979(1, 2)	1.9422(1, 3)	1.9648(1, 5)	1.9422(1, 6)	1.9422(1, 9)	2.8554 (4, 15)
	10	1.9358(1, 2)	1.6596(1, 3)	1.6951(1, 4)	1.6596(1, 6)	1.6596(1, 9)	2.4217 (4, 15)
1000							
	0	3.9291(1, 2)	3.9291(1, 4)	3.8012(1, 5)	3.7887(1, 7)	3.8012(1, 10)	5.7058 (5, 15)
	1	2.1137(1, 2)	2.1137(1, 4)	2.1049(1, 5)	2.0820(1, 7)	2.0773(1, 11)	3.1296 (5, 15)
	5	1.2943(1, 2)	1.2865(1, 3)	1.2451(1, 5)	1.2432(1, 7)	1.2451(1, 10)	1.8510 (5, 15)
	10	1.1270(1, 2)	1.0850(1, 3)	1.0623(1, 5)	1.0665(1, 7)	1.0623(1, 10)	1.5850 (5, 15)
1200							
	0	2.6407(1, 2)	2.6407(1, 4)	2.6407(1, 6)	2.6407(1, 8)	2.6385(1, 11)	4.0515 (6, 15)
	1	1.4428(1, 2)	1.4428(1, 4)	1.4428(1, 6)	1.4428(1, 8)	1.4428(1, 12)	2.1942 (6, 15)
	5	0.8682(1, 2)	0.8682(1, 4)	0.8682(1, 6)	0.8682(1, 8)	0.8650(1, 11)	1.3167 (6, 15)
	10	0.7480(1, 2)	0.7480(1, 4)	0.7480(1, 6)	0.7411(1, 7)	0.7379(1, 11)	1.1169 (5, 15)
1500							
	0	1.6978(1, 2)	1.6978(1, 4)	1.6978(1, 6)	1.6908(1, 9)	1.6833(1, 12)	2.6098 (6, 15)
	1	0.9453(1, 2)	0.9453(1, 4)	0.9269(1, 7)	0.9237(1, 9)	0.9253(1, 12)	1.4259 (7, 15)
	5	0.5565(1, 2)	0.5565(1, 4)	0.5565(1, 6)	0.5563(1, 9)	0.5532(1, 12)	0.8457 (6, 15)
	10	0.4732(1, 2)	0.4732(1, 4)	0.4732(1, 6)	0.4732(1, 8)	0.4732(1, 13)	0.7208 (6, 15)

The critical buckling loads q_{cr} (MPa) increases when the ratio r_1/R increases but there is no definite trend of variation of critical loads versus various values of r_0/R. When r_0/R increases, the critical buckling load decreases, the abnormal trend occurs when the ratio r_0/R nearly approaches the ratio r_1/R. In this case, the width annular spherical segments is narrow. These results are presented in the Table 6.

Table 6. Effects of ratios r_o/R and r_1/R on the critical buckling loads q_{cr} x10^1 (MPa) of annular spherical segments under radial pressure $\left(k=1,\ R/h=1000,\ \beta=45^o\right)$

r_0/R	r_1/R				
	0.3	0.35	0.4	0.45	0.5
0.1	2.2266 (1, 3)	2.4355 (1, 4)	2.5012 (1, 4)	2.6685 (1, 5)	2.6561 (7, 2)
0.15	1.9484 (1, 3)	2.0236 (1, 4)	2.1506 (1, 4)	2.2643 (1, 5)	2.3620 (1, 5)
0.2	1.9003 (1, 4)	1.8118 (1, 4)	1.9111 (1, 5)	1.9768 (1, 5)	2.1049 (1, 5)
0.25	3.2849 (1, 5)	1.8708 (1, 4)	1.7447 (1, 5)	1.7971 (1, 5)	1.8738 (1, 6)

The critical buckling loads for FGM annular spherical segments under simultaneous action of compressive load and radial pressure are displayed in Table 7 for different combinations of geometry parameters.

Table 7. Critical buckling loads (q_{cr} x 10^4, p_{cr}) (GPa) of annular spherical segments under combination of compressive load and radial pressure $\left(k=1,\ R/h=1000, \gamma=p_{cr}/q_{cr}\right)$

$\beta\left(^o\right)$	γ	$\left(r_0/R,\ r_1/R\right)$		
		(0.1, 0.3)	(0.15, 0.4)	(0.2, 0.5)
30				
	0	(2.2266, 0)	(2.1465, 0)	(2.1137, 0)
	500	(2.5919, 0.1296)	(2.5497, 0.1275)	(2.5324, 0.1266)
	2000	(1.9034, 0.3807)	(1.6494, 0.3299)	(1.5206, 0.3041)
	$+\infty$	(0, 1.0695)	(0, 0.7006)	(0, 0.5709)
45				
	0	(2.2266, 0)	(2.1506, 0)	(2.1049, 0)
	500	(2.5411, 0.1271)	(2.5253, 0.1263)	(2.5189, 0.1259)
	2000	(1.7476, 0.3495)	(1.5656, 0.3131)	(1.4688, 0.2938)
	$+\infty$	(0, 0.8395)	(0, 0.6180)	(0, 0.5285)
60				
	0	(2.2266, 0)	(2.1465, 0)	(2.0820, 0)
	500	(2.5262, 0.1263)	(2.5182, 0.1259)	(2.5148, 0.1257)
	2000	(1.6964, 0.3393)	(1.5374, 0.3075)	(1.4511, 0.2902)
	$+\infty$	(0, 0.7746)	(0, 0.5921)	(0, 0.5146)

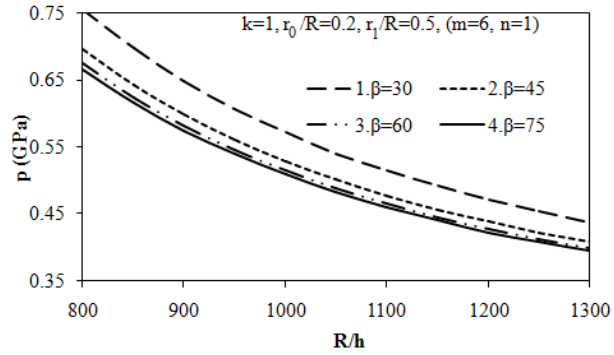

Fig. 2. Effects of ratio R/h to the buckling loads of the annular spherical segments under compressive load

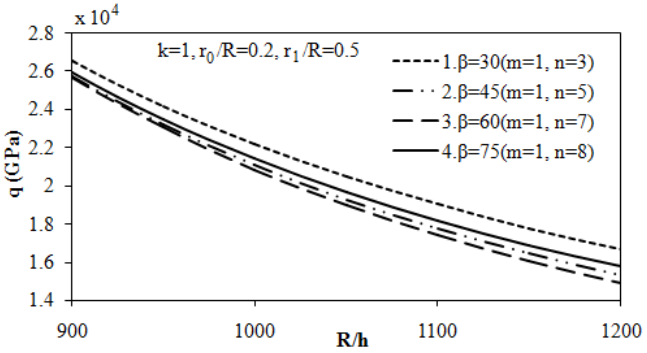

Fig. 3. Effects of ratio R/h on the buckling loads of annular spherical segments under radial pressure

Next, the variation of buckling compressive and pressure load versus R/h ratio is separately illustrated in Fig.2 and 3. As can be observed, there is a considerable difference between buckling loads with small R/h ratio. In contrast, this difference becomes small when R/h ratio to be larger.

Finally, the variation trend of the buckling compressive loads versus r_1/R ratio is presented in Fig. 4. The results show that buckling curves to be lower with increasing values of open and these curves exits the minimal points when r_1/R ratio increases.

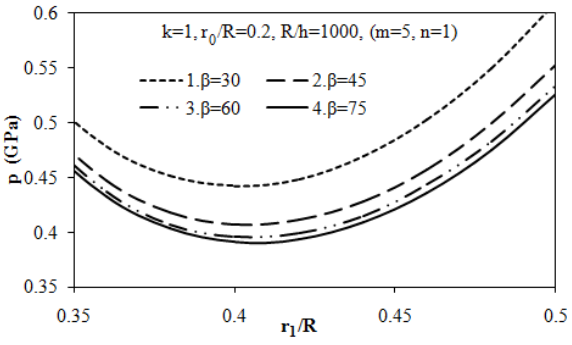

Fig. 4. Effects of ratio r_1/R on the buckling loads of annular spherical segments under compressive load.

5. Conclusions

The present paper aims to propose an analytical approach to investigate the linear buckling of simply supported FGM annular spherical segments subjected to mechanical loads. Formulation is based on the classical the shell theory and the adjacent equilibrium criterion.

Approximate solutions are assumed to satisfy the simply supported boundary conditions and Galerkin method is applied to derive the closed form relations of buckling load. Buckling behavior of FGM annular spherical segments can be investigated. Some effects of material and dimensional parameters to the buckling of FGM annular spherical segments are observed, that illustrates specified characteristics of this structure.

The study shows that

+ There exist a definite trend of variations of critical compressive and pressure loads versus variation values of open angle β, volume fraction index k and ratio R/h.

+ Variation trend of the critical compression versus ratios r_0/R and r_1/R is stable but that of the critical pressure is not stable.

+ Buckling behavior of FGM annular spherical segments is complex and very sensitive to variation of material and geometrical parameters.

Acknowledgements

This research is funded by Vietnam National Foundation for Science and Technology Development (NAFOSTED) under grant number 107.02-2013.02.

Appendix A

$$l_{11}(u)=E_1\left[\frac{\partial^2}{\partial r^2}+\frac{1}{r}\frac{\partial}{\partial r}-\frac{1}{r^2}+\frac{1-\nu}{2r^2}\frac{\partial^2}{\partial\theta^2}\right],$$

$$l_{12}(v)=E_1\left[\frac{1+\nu}{2r}\frac{\partial^2}{\partial r\partial\theta}-\frac{3-\nu}{2r^2}\frac{\partial}{\partial\theta}\right],$$

$$l_{13}(\mathrm{w})=-E_2\left[\frac{\partial^3}{\partial r^3}+\frac{1}{r}\frac{\partial^2}{\partial r^2}-\frac{1}{r^2}\frac{\partial}{\partial r}-\frac{1-\nu}{r^2}\frac{\partial^2}{\partial r\partial\theta}+\frac{1}{r^2}\frac{\partial^3}{\partial r\partial\theta^2}-\frac{1+\nu}{r^3}\frac{\partial^2}{\partial\theta^2}\right]-\frac{1+\nu}{R}E_1\frac{\partial}{\partial r},$$

$$l_{21}(u)=E_1\left[\frac{1+\nu}{2r}\frac{\partial^2}{\partial r\partial\theta}+\frac{3-\nu}{2r^2}\frac{\partial}{\partial\theta}\right],$$

$$l_{22}(v)=E_1\left[-\frac{1-\nu}{2r^2}+\frac{1-\nu}{2r}\frac{\partial}{\partial r}+\frac{1-\nu}{2}\frac{\partial^2}{\partial r^2}+\frac{1}{r^2}\frac{\partial^2}{\partial\theta^2}\right],$$

$$l_{23}(\mathrm{w})=-E_2\left[\frac{1}{r^3}\frac{\partial^3}{\partial\theta^3}+\frac{1}{r}\frac{\partial^3}{\partial r^2\partial\theta}+\frac{2-\nu}{r^2}\frac{\partial^2}{\partial r\partial\theta}-\frac{1-\nu}{r}\frac{\partial^2}{\partial r^2}-\frac{1-\nu}{r^2}\frac{\partial}{\partial r}\right]-\frac{1+\nu}{Rr}E_1\frac{\partial}{\partial\theta},$$

$$l_{31}(u)=E_2\left[\frac{\partial^3}{\partial r^3}+\frac{2}{r}\frac{\partial^2}{\partial r^2}-\frac{1}{r^2}\frac{\partial}{\partial r}+\frac{1}{r^3}+\frac{1}{r^2}\frac{\partial^3}{\partial r\partial\theta^2}+\frac{1}{r^3}\frac{\partial^2}{\partial\theta^2}\right]+\frac{1+\nu}{R}E_1\left(\frac{\partial}{\partial r}+\frac{1}{r}\right),$$

$$l_{32}(v)=E_2\left[\frac{1}{r}\frac{\partial^3}{\partial r^2\partial\theta}-\frac{1}{r^2}\frac{\partial^2}{\partial r\partial\theta}+\frac{1}{r^3}\frac{\partial}{\partial\theta}+\frac{1}{r^3}\frac{\partial^3}{\partial\theta^3}\right]+\frac{1+\nu}{Rr}E_1\frac{\partial}{\partial\theta},$$

$$l_{33}(\mathrm{w})=-E_3\left[\frac{\partial^4}{\partial r^4}+\frac{2}{r}\frac{\partial^3}{\partial r^3}+\frac{2}{r^2}\frac{\partial^4}{\partial r^2\partial\theta^2}-\frac{2(1-\nu)}{r^2}\frac{\partial^3}{\partial r^2\partial\theta}-\frac{2\nu}{r^3}\frac{\partial^3}{\partial r\partial\theta^2}-\frac{1}{r^2}\frac{\partial^2}{\partial r^2}+\frac{1}{r^3}\frac{\partial}{\partial r}+\right.$$
$$\left.+\frac{2(1+\nu)}{r^4}\frac{\partial^2}{\partial\theta^2}+\frac{1}{r^4}\frac{\partial^4}{\partial\theta^4}\right]-\frac{2(1+\nu)}{R}E_2\left[\frac{\partial^2}{\partial r^2}+\frac{1}{r}\frac{\partial}{\partial r}+\frac{1}{r^2}\frac{\partial^2}{\partial\theta^2}\right]-\frac{2(1+\nu)}{R^2}E_1,$$

$$l_{34}=-\frac{(1-\nu^2)R}{2}\left[\frac{r^2+r_0^2}{r^4}\frac{\partial^2}{\partial\theta^2}+\frac{r^2+r_0^2}{r^3}\frac{\partial}{\partial r}+\frac{r^2-r_0^2}{r^2}\frac{\partial^2}{\partial r^2}\right],$$

$$l_{35}=-(1-\nu^2)h\left[\frac{r_0^2}{r^2}\frac{\partial^2}{\partial r^2}-\frac{r_0^2}{r^4}\frac{\partial^2}{\partial\theta^2}-\frac{r_0^2}{r^3}\frac{\partial}{\partial r}\right].$$

Appendix B

$$a_{11}=\frac{m^2\pi^2(1-\lambda^4)}{8(1-\lambda)^2}+\frac{1-\lambda^2}{8}\left[3+(1-\nu)\left(\frac{n\pi}{\beta}\right)^2\right],$$

$$a_{12}=\frac{1+\nu}{12}\frac{mn\pi^2(1-\lambda^3)}{\beta(1-\lambda)}+\frac{n(1-\lambda)^2}{2m\beta},$$

$$a_{13}=-\frac{\overline{E_2}\delta}{\overline{E_1}}\left[\frac{m^3\pi^3(1-\lambda^4)}{8(1-\lambda)^3}+\frac{3m\pi(1-\lambda^2)}{8(1-\lambda)}+\frac{mn^2\pi^3(1-\lambda^2)}{4\beta^2(1-\lambda)}\right]+$$
$$+\frac{\xi(1+\nu)}{8}\left[\frac{m\pi(1-\lambda^4)}{(1-\lambda)}+\frac{3(1-\lambda)(1-\lambda^2)}{m\pi}\right],$$

$$a_{21}=\frac{1+\nu}{12}\frac{mn\pi^2(1-\lambda^3)}{\beta(1-\lambda)}+\frac{n(1-\nu)(1-\lambda)^2}{4m\beta},$$

$$a_{22}=\frac{(1-\nu)(1-\lambda^2)}{16}+\frac{m^2\pi^2(1-\nu)(1-\lambda^4)}{16(1-\lambda)^2}+\frac{n^2\pi^2(1-\lambda^2)}{4\beta^2},$$

$$a_{23}=-\frac{\overline{E_2}\delta}{\overline{E_1}}\left[\frac{n^3\pi^3(1-\lambda)}{2\beta^3}+\frac{nm^2\pi^3(1-\lambda^3)}{6\beta(1-\lambda)^2}+\frac{n\pi(1-\nu)(1-\lambda)}{4\beta}\right]+$$
$$+\xi(1+\nu)\left[\frac{n\pi(1-\lambda^3)}{6\beta}-\frac{n(1-\lambda)^3}{4\beta m^2\pi}\right],$$

$$a_{31}=\frac{\overline{E_2}\delta}{\overline{E_1}}\left[\frac{m^3\pi^3\left(1-\lambda^5\right)}{10(1-\lambda)^3}+\frac{mn^2\pi^3\left(1-\lambda^3\right)}{6\beta^2(1-\lambda)}-\frac{(1-\lambda)^2}{2m\pi}+\frac{m\pi\left(1-\lambda^3\right)}{6(1-\lambda)}\right]-$$

$$-\xi(1+\nu)\left[\frac{m\pi\left(1-\lambda^5\right)}{10(1-\lambda)}-\frac{(1-\lambda)\left(1-\lambda^3\right)}{4m\pi}+\frac{3(1-\lambda)^4}{8m^3\pi^3}\right],$$

$$a_{32}=\frac{\overline{E_2}\delta}{\overline{E_1}}\left[\frac{nm^2\pi^3\left(1-\lambda^4\right)}{8\beta(1-\lambda)^2}-\frac{7n\pi\left(1-\lambda^2\right)}{8\beta}+\frac{n^3\pi^3\left(1-\lambda^2\right)}{4\beta^3}\right]+$$

$$+\xi(1+\nu)\left[\frac{3n(1-\lambda)^2\left(1-\lambda^2\right)}{8\beta m^2\pi}-\frac{n\pi\left(1-\lambda^4\right)}{8\beta}\right],$$

$$a_{33}=-\frac{\overline{E_3}\delta^2}{\overline{E_1}}\left[\frac{m^4\pi^4\left(1-\lambda^5\right)}{10(1-\lambda)^4}+\frac{m^2n^2\pi^4\left(1-\lambda^3\right)}{3\beta^2(1-\lambda)^2}-\frac{3n^2\pi^2(1+\nu)(1-\lambda)}{2\beta^2}+\frac{m^2\pi^2\left(1-\lambda^3\right)}{6(1-\lambda)^2}-\right.$$

$$\left.-\frac{(1-\lambda)}{2}+\frac{n^4\pi^4(1-\lambda)}{2\beta^4}\right]-(1+\nu)\xi^2\left[\frac{\left(1-\lambda^5\right)}{5}-\frac{(1-\lambda)^2\left(1-\lambda^3\right)}{m^2\pi^2}+\frac{3(1-\lambda)^5}{2m^4\pi^4}\right]+$$

$$+(1+\nu)\frac{\overline{E_2}\delta\xi}{\overline{E_1}}\left[\frac{m^2\pi^2\left(1-\lambda^5\right)}{5(1-\lambda)^2}-\frac{\left(1-\lambda^3\right)}{2}+\frac{3(1-\lambda)^3}{4m^2\pi^2}+\frac{n^2\pi^2\left(1-\lambda^3\right)}{3\beta^2}-\frac{n^2(1-\lambda)^3}{2\beta^2m^2}\right],$$

$$a_{34}=\frac{\left(1-\nu^2\right)}{4\delta\xi}\left[\frac{n^2\pi^2\left(1-\lambda^3\right)}{3\beta^2}-\frac{n^2(1-\lambda)^3}{2\beta^2m^2}+\frac{n^2\pi^2\lambda^2(1-\lambda)}{\beta^2}-\frac{\left(1-\lambda^3\right)}{2}+\frac{3(1-\lambda)^3}{4m^2\pi^2}+\right.$$

$$\left.+\lambda^2(1-\lambda)+\frac{m^2\pi^2\left(1-\lambda^5\right)}{5(1-\lambda)^2}-\frac{m^2\pi^2\lambda^2\left(1-\lambda^3\right)}{3(1-\lambda)^2}\right],$$

$$a_{35}=\frac{\left(1-\nu^2\right)\lambda^2}{2}\left[\frac{m^2\pi^2\left(1-\lambda^3\right)}{3(1-\lambda)^2}-\left(\frac{n^2\pi^2}{\beta^2}+1\right)(1-\lambda)\right]$$

where

$$\lambda=\frac{r_0}{r_1},\ \xi=\frac{r_1}{R},\ \delta=\frac{h}{r_1},\ \overline{E_1}=\frac{E_1}{h},\ \overline{E_2}=\frac{E_2}{h^2},\ \overline{E_3}=\frac{E_3}{h^3},q^*=\frac{q}{\overline{E_1}},\ p^*=\frac{p}{\overline{E_1}}.$$

References

[1] Budiansky B, Roth RS. Axisymmetric dynamic buckling of clamped shallow spherical shells, NASA TND 1962; 510: 597–609.

[2] Huang NC. Unsymmetrical buckling of thin shallow spherical shells. J Appl Mech Trans ASME 1964; 31: 447–457.

[3] Tillman SC, On the buckling behavior of shallow spherical caps under a uniform pressure load. Int J Solids Struct1970; 6:37–52.

[4] Ball R, Burt JA. Dynamic buckling of shallow spherical shells. ASME J Appl Mech 1973; 41: 411–416.

[5] Kao R, Perrone N. Dynamic buckling of axisymmetric spherical caps with initial imperfection. Comput Struct 1978; 9:463–473.

[6] Ganapathi M, Varadan TK, Dynamic buckling of orthotropic shallow spherical shells, Comput Struct 1982; 15:517–520.

[7] Dumir PC, Nonlinear axisymmetric response of orthotropic thin spherical caps on elastic foundations, Int J Mech Sci 1985; 27: 751–760.

[8] Chao CC, Lin IS. Static and dynamic snap-through of orthotropic spherical caps. Compos Struct 1990; 14: 281–301.

[9] Xu CS. Buckling and post-buckling of symmetrically laminated moderately thick spherical caps. Int J Solids Struct 1991; 28:1171–1184.

[10] Muc A, Buckling and postbuckling behavior of laminated shallow spherical shells subjected to external pressure. Int J Nonlinear Mech 1992; 27(3):465–476.

[11] Ganapathi M, Varadan TK. Dynamic buckling of laminated anisotropic spherical caps. J Appl Mech 1995; 62:13–19.

[12] Dube GP, Joshi S, Dumir PC. Nonlinear analysis of thick shallow spherical and conical orthotropic caps using Galerkin's method. Appl Math Modelling 2001;25:755–773.

[13] Nie GH, Asymptotic buckling analysis of imperfect shallow spherical shells on non-linear elastic foundation. Int J Mech Sci 2001;43:543–555.

[14] Eslami MR, Ghorbani HR, Shakeri M. Thermoelastic buckling of thin spherical shells. J Therm Stresses 2001:24:1177–1198.

[15] Shahsiah R, Eslami MR. Thermal and mechanical instability of an imperfect shallow spherical cap. J Therm Stresses 2003;26(7):723–737.

[16] Wunderlich W, Albertin U. Buckling behavior of imperfect spherical shells. Int J Nonlinear Mech 2002; 37:589–604.

[17] Li QS, Liu J, Tang J. Buckling of shallow spherical shells including the effects of transverse shear deformation. Int J Mech Sci 2003; 45:1519–1529.

[18] Shahsiah R, Eslami MR, Naj R. Thermal instability of functionally graded shallow spherical shell. J Therm Stresses 2006; 29(8):771–790.

[19] Prakash T, Sundararajan N, Ganapathi M. On the nonlinear axisymmetric dynamic buckling behavior of clamped functionally graded spherical caps. J. Sound Vibrat 2007; 299:36–43.

[20] Ganapathi M. Dynamic stability characteristics of functionally graded materials shallow spherical shells. Compos Struct 2007;79:338–343.

[21] Bich DH. Nonlinear buckling analysis of FGM shallow spherical shells. Vietnam J Mech 2009; 31:17–30.

[22] Bich DH, Hoa LK. Nonlinear vibration of functionally graded shallow spherical shells. Vietnam J Mech 2010; 32:199–210.

[23] Bich DH, Tung HV. Nonlinear axisymmetric response of functionally graded shallow spherical shells under uniform external pressure including temperature effects. Int J Nonlinear Mech 2011;46:1195–1204.

[24] Shahsiah R, Eslami MR, Sabzikar Boroujerdy M. Thermal instability of functionally graded deep spherical shell. Arch Appl Mech2011; 81:1455–1471.

[25] Bich DH, Dung DV, Hoa LK. Nonlinear static and dynamic buckling analysis of functionally graded shallow spherical shells including temperature effects. Compos Struct 2012;94:2952-2960.

[26] Aghdam MM, Shahmansouri N, Bigdeli K. Bending analysis of moderately thick functionally graded conical panels. Compos Struct 2011; 93:1376–1384.

[27] Bich DH, Phuong NT, Tung HV. Buckling of functionally graded conical panels under mechanical loads. Composite Structures 2012;94:1379–1384.

[28] Brush DO, Almroth BO. Buckling of Bars, Plates and Shells. McGraw-Hill, New York, 1975.

[29] Timoshenko SP, Gere JM. Theory of elastic stability. McGraw-Hill, New York, 1961.

[30] Paczos P, Zielnica J. Stability of orthotropic elastic–plastic open conical shells. Thin-Walled Structures 2008; 46:530-540.